AN S1S WAVEGUIDE HETERODYNE RECEIVER FOR 600 GHz -635 GHz

Morvan Salez, Pascal **Febvre*,** William **R. McGrath,**
Bruce Bumble, henry G. **LeDuc**

Jet Propulsion Laboratory -
Center for Space Microelectronics Technology
4800 Oak Grove Drive, Pasadena, California 91109
**DEMIRM-Observatoire de Meudon, 92195 Meudon Cedex, France*

Abstract

A waveguide S1S heterodyne receiver using a Nb/AlO_x/Nb junction has been built for astronomical observations of molecular transitions in the frequency range 600 GHz -635 GHz, and has been successfully used at the Caltech Submillimeter Observatory (CSO). We report double sideband (DSB) receiver noise temperatures as low as 245 K at 600 GHz - 610 GHz, and near 300 K over the rest of the. bandwidth, These results confirm that S1 S quasi particle. mixers work well at submillimeter-wave frequencies corresponding to photon energies of at least 9(F% of the. superconductor energy gap. In addition, we have systematically investigated the. effect on the receiver performance. of the overlap between first-order and second-order photon steps of opposite sign at these frequencies. The receiver noise increases by as much as 40% in the region of overlap. We infer potential limitations for operating submillimeter-wave Nb/AlO_x/Nb mixers.

Key words: superconductors; S1S junctions; S1S mixers; S1S receivers; submillimeter waves.

1. Introduction

The most sensitive heterodyne receivers at millimeter and submillimeter wavelengths have made use of quasiparticle S 1 S (Superconductor-insulator-Superconductor) mixers [1-4]. The mixing response originates from the. highly nonlinear tunneling currents in these devices, and quantum mixer theory predicts both high RF-to-IF conversion gain and quantum-limited noise [S]. Several receivers are currentl y operated on telescopes at frequencies approaching S00 GHz [1,2,6], and the use of S1S mixers at still higher frequencies has been demonstrated in the laboratory [3,4,7]. in this article, we describe a waveguide S1S receiver, employing a $Nb/AlO_x/Nb$ tunnel junction, for use in the frequency range 600 GI lz 635 GI l z. One of the primary objectives is the detection of the 625.9 GHz ground-state rotational transition line of HC1, both in the atmosphere of Venus and in the dense. regions of interstellar molecular clouds. 'l"his receiver has been characterized in the laboratory and used at the Caltech Submillimeter Observatory (CSO) in 1 lawaii.

2. Receiver Description

2.1. Junction Fabrication

The submicron-area $Nb/AlO_x/Nb$ junctions are fabricated from a D C-sputtered trilayer using electron-beam lithography with a self-aligned insulator lift-off technique [8]. The base and top electrodes are respective] y 1600 Å ant] 2300 Å thick. The DC and IF electrodes, which include the. RF choke. filter, arc defined by conventional photolithography. "l'he. critical cur-rent density of the junction used in this receiver is approximately 11 kA/cm^2 and the surface area is $(0.5 \times 0.5)\ \mu m^2$. The normal resistance R_N at 4.2. K is 73 Ω. The capacitance, per unit area is estimated to be (80 - 100) $fF/\mu m^2$ and is strongly dependent cm the critical current density. All junctions arc fabricated *cm 1()()-pm* thick quartz wafers, which are later lapped and diced into 50-μm thick and 100-μm wide individual substrates.

2.2 Integrated Tuning Circuits

A superconductive RF tuning circuit is integrated with the junction to improve. the RF impedance match. This microstrip circuit uses one side of the. choke filter as a ground plane, and the junction counter electrode,

extending on top of the 2000-Å thick SiO dielectric, as the microstrip. The tunnel junction has a susceptance $j\omega C$ at an angular frequency ω, due. to the geometric capacitance C. This capacitive, susceptance competes with the nonlinear quasiparticle conductance. used by the mixer, and the quantity $\omega R_N C$ is an approximate measure of the ratio of the two admittances and of the mixer instantaneous bandwidth. At high signal frequencies, the capacitance shunts the mixer. Reducing, C can be achieved by producing smaller junctions. However, $\omega R_N C$ is still typically much larger than 1 in the. submillimeter-wave range, and the. capacitance must be tuned out for optimum mixer performance.. The junction described in this article is characterized by $\omega R_N C \sim 6$-7 at 600 GHz.

A distributed inductance - $1/\omega^2 C$ has been integrated in parallel with the junction, in order to resonate out the capacitance at the signal frequency. This inductance is provided by a superconductive Nb/SiO/Nb microstrip circuit strongly coupled to the. junction. This technique has been successful] y used at several lower frequencies [4,7,9,10]. For a single-section tuning circuit, the mixer performance is improved over an RF bandwidth which depends inversely on its quality factor and can bc as narrow as 5 % at the -] 0 dB return loss level. Since multisection resonant circuits are expected to have. a broader bandwidth, we have designed and tested several circuits, with either one or two sections, We describe here one. particular circuit design that has proved to work well: a quarter-wavelength radial stub used in combination with a short section of transmission line (see Fig. 1). The 900 radial stub provides a wide-band RF short [1 1]. This short is then transformed into the appropriate inductance by a 25-μm long, 5-μm wide transmission line, of characteristic impedance $Z_0 \approx 8.5\ \Omega$. A similar design which uses a quarter-wavelength straight microstrip line. as the RF short has also been tested.

Due to the penetration of magnetic fields in the superconducting electrodes, a Nb/SiO/Nb microstrip line is a slow-wave transmission line, and its phase. velocity is

$$v_p = c / \sqrt{\varepsilon_r \mu_{eff}} \sim 0.27\ c \qquad (1)$$

where c is the speed of light in vacuum, ε_r is the relative dielectric constant of SiO estimated to be 5.S, and $\mu_{eff} = 1 + (\lambda/d)(\coth(t_1/\lambda) + \coth(t_2/\lambda)) > 1$ is an effective, relative magnetic permeability which takes into account this penetration effect [12, 13]: t_1 and t_2 are. respectivel y the. thicknesses of the

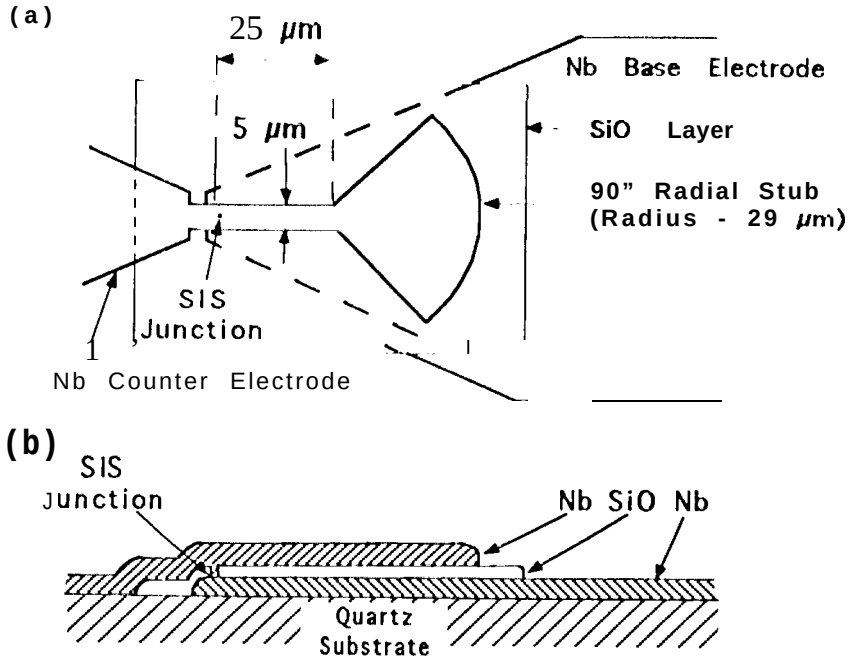

Fig. 1. Top (a) and cross-section (b) views (not (o scale) of the microstrip Nb/SiO/Nb tuning circuit coupled to the junction. 'l'he radial stub provides a broadband RF short at the end of the transmission line.

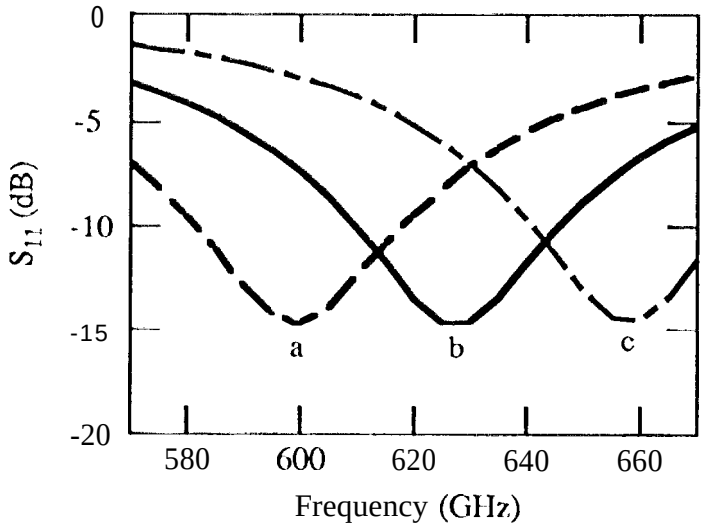

Fig. 2. Calculated S_{11} parameter versus signal frequency, for the tuning circuit of Fig. 1, assuming $Z_S = 50\ \Omega, Cj = 21$ fF, and (a) $\lambda = 900$ Å; (b) $\lambda = 750$ Å; (c) $\lambda = 600$ Å.

lower and upper electrodes, d is the SiO dielectric thickness and λ is the magnetic penetration depth in Nb, estimated to be 7S() Å [14]. For a microstrip line of width w, the characteristic admittance can be written

$$Y_0 = 1/(1207c)\ K\,(w/d)\sqrt{\varepsilon_r/\mu_{eff}} \qquad (2.)$$

where κ is a fringing factor calculated to be between 1.05 and 1.35 for our our geometry [15]. Similarly, the radial stub dimensions have been calculated with an effective relative magnetic permeability which accounts for the magnetic penetration depth of the. superconductors. In these calculations, however, potential dispersion in the microstrip structure has not been considered. In Fig. 2, the s_{11} parameter is plotted versus frequency, for the junction and integrated circuit of Fig. 1 coupled to a 50-Ω source impedance, This source impedance is typical of what is readily achieved by the waveguide mixer circuit. As can be seen, the signal power is expected to be coupled into the junction over a bandwidth of about 30 GHz at the -1 0-dB level.

2.3 Mixer Block

The mixer consists of the. S1S tunnel junction with the integrated superconductive circuit, placed in a waveguide mount, as shown in Fig.3. The waveguide dimensions are 170 µm x 366 pm which results in a frequency band of 410 GHz - 820 GHz for the TE_{10} mode. The Slli>rllil]irllcler-wave. radiation is coupled into this waveguide via a dual-mode conical feedhorn, characterized by very low sidelobe levels and nearly equal E and H plane. patterns [16]. 'l"he. substrate, is mounted across the rectangular waveguide along the. E-field direction. It is held in place in a 135-µm wide channel by a very thin film of cyanoacrylate glue.. The two ends of the RF choke filter are wire-bonded respectively to the mixer block (ground) and to the central pin of the IF output coaxial connector, using 25-pm diameter aluminum wire. Two identical mixer blocks have been used. For the first one. (refered m hereafter as "M 1 "), the horn was electroformed by Custom Microwaves [17], while the mixer block was machined and gold-plated in house. The second block (M2) was entirely manufactured by Radiometer Physics.

The purpose. of the waveguide mount, designed using a low-frequency (4 GHz - 6 GHz) model [18], is to provide the match to the real part of the junction impedance, but also an inductive. susceptance, should the RF microstrip circuit not fully compensate the junction capacitance. For this, two adjustable tuning elements are. employed, a backshort, and an E-

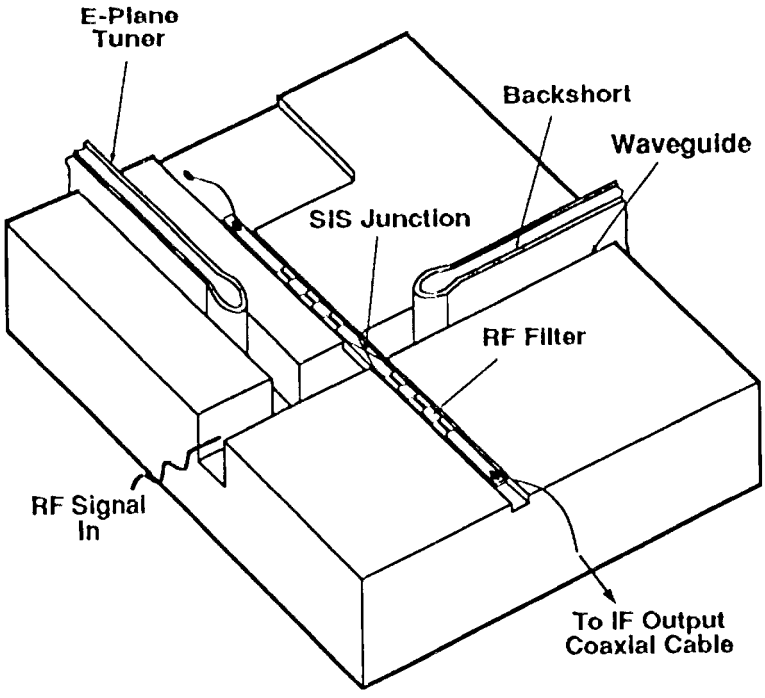

Fig. 3. Perspective drawing of the mixer block, when the horn and the IF output connector have been removed.

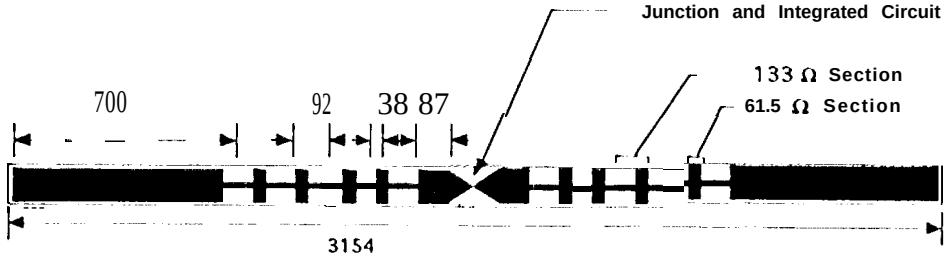

Fig. 4. Drawing of the 50-μm thick, 100-μm wide quartz substrate and of the Nb/AlO_x/Nb junction electrodes, designed to provide a microstrip RF choke filter (all dimensions in microns).

plane. tuner located about one guide wavelength (635 pm) away from the substrate channel. Both tuners are of the contacting type, and use gold-plated BeCu strips, folded on themselves as tight springy loops. This technique has proved to work well at many frequencies. The junction electrodes constitute a symmetrical RF choke filter, shown in Fig. 4, which prevents the RF signal from leaking out of the waveguide through the bias/IF leads. This microstrip filter, which consists of a series of high and low impedance sections, was initially designed to provide an RF short at the waveguide wall. Subsequently, the length of the first low-impedance section has been increased and the. taper angle of the. metallization in the waveguide adjusted from 90° to 45°, in order to minimize the forbidden region and move it toward the high impedance, side. of the Smith chart. q-he overall tunable. bandwidth is determined primarily by the relatively large substrate. channel, and is expected to be about 20%.

A coil of superconducting NbTi wire, in the vicinity of the junction, produces a magnetic field aligned with the junction plane that averages out the Josephson currents. These currents, in various ways, are a source of noise in a quasiparticle mixer. The 6000-turn coil surrounds the. mixer block and is capable of generating up to 1000 Gauss, This is sufficient to apply at least three. magnetic flux quanta within the junction since, given the junction dimension of 0.5 pm and the estimated penetration depth of 750 Å, the. magnetic field corresponding to one flux quantum (2×10^{-15} Wb) is about 300 Gauss.

2.4. Optics

The local oscillator (J .O) consists of a 100 GHz - 106 GHz Gunn source. followed by x2x3 whi sker-contacted Schot tk y varactor mult ipliers [19]. The feed horn on the. multiplier is identical to that described above for the mixer. A harmonic mixer with an internal -10-dB coupler [20] is inserted between the. Gunn oscillator and the multipliers to make a reference. signal available for a phase-lock system.

The LO and RF signals arc diplexed via a 12.5-yin mylar beamsplitter at an angle of 45° with both optical paths, and enter the cryostat through a 25-μm thick mylar vacuum-tight window. The combined beam is focused onto the mixer feedhorn by an off-axis elliptical mirror (see Fig. 5). The use of elliptical mirrors solves the problems of reflection and of increasing absorptivity of dielectric lenses at shorter wavelengths. These mirrors have been designed assuming a beam waist of 0.9 mm for the horn ($w = 1.78\ \lambda_0$), and a 2.2-mm beam waist for the f/6 Cassegrain telescope

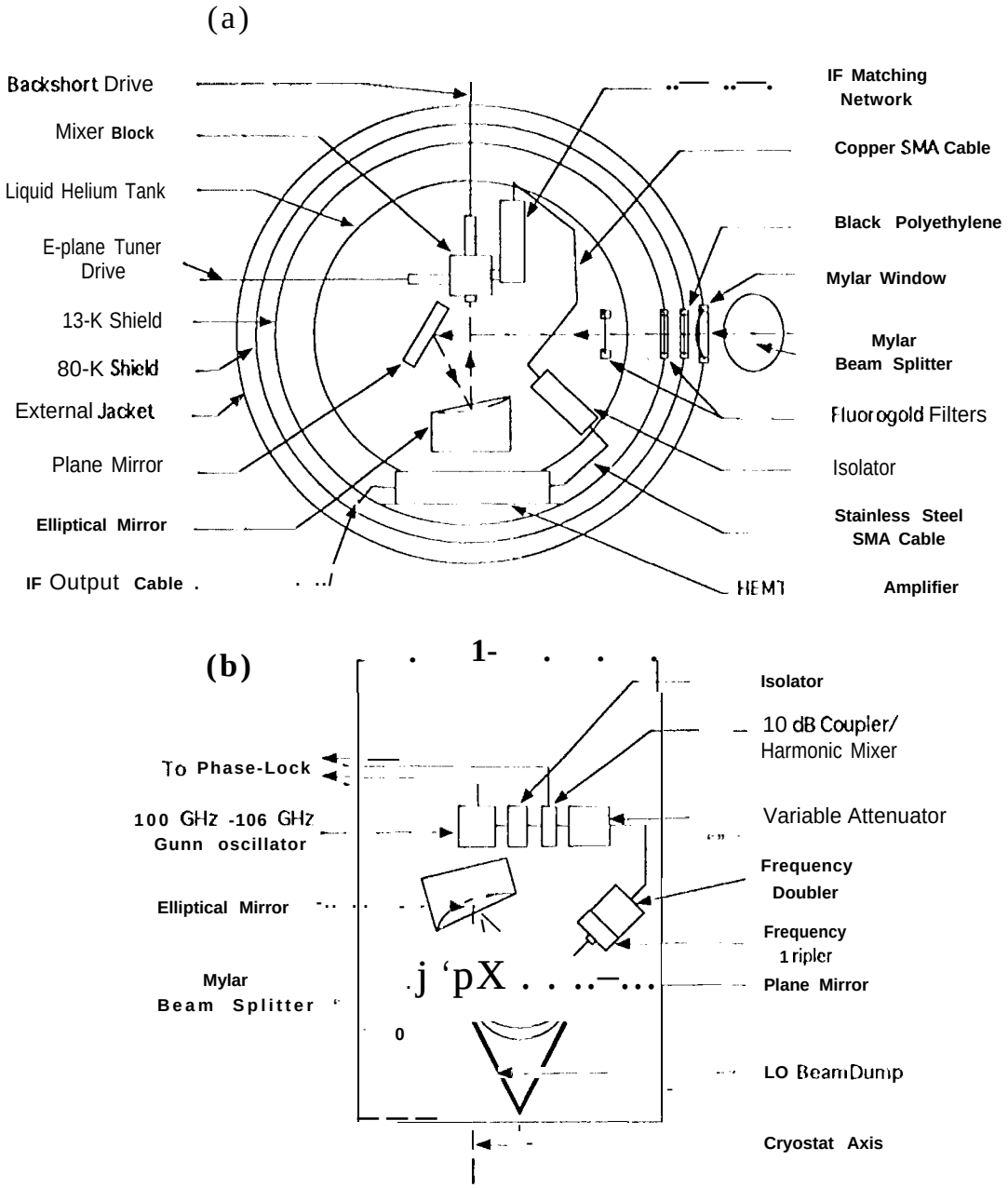

Fig. 5. Schematic drawing of the receiver, showing the optics layout both inside the cryostat (a) and on the external LO plate (b). Dashed lines trace the optical path.

beam. This approximately corresponds to a 10-dB edge taper on the telescope primary reflector, according to:

$$T(\mathrm{dB}) = 20.66\ [w / (f_E/D_m)\,\lambda)]^2 \qquad (3)$$

where f_E is the effective focal length of the telescope and D_m the diameter of its main reflector [21]. This value of the edge taper is a good tradeoff between spillover losses and beam efficiency, which tend to respectively decrease and saturate for an increasing edge taper. The divergence angle of the beam, defined by the $1/e$ electric field contour of the beam in far field, is 19.4° at the mixer dual-mode horn, and 7.8° outside. the. cryostat.

in the cryostat, three infrared filters are. placed across the optical path on the various radiation shields. They shield the inner parts of the cryostat from most of the room temperature. radiation, hence avoiding both a reduction of the cryostat hold-time and a possible mixer saturation. In addition, the circular apertures of these filters limit the field of view to a half angle of 18°. A 50-μm thick black polyethylene window at 80 K, and two *fluorogold* resonant filters (one wavelength thick) at 13 K and 4.2 K are currently used, For reflection and transmission calculations, the dielectric constants near 630 GHz for mylar, fluorogold and polyethylene were taken equal to 3, 2.56 and 2.14 respectively [2.1,22]. The beamsplitter has a calculated transmission of 97%, and its walkoff is 36 μm, which is negligible compared to the. local size of the beam (1 .92 mm).

All elliptical mirrors have been machined with a digital lathe, achieving a surface accuracy of $\lambda/35$. Finer polishing has made it possible to align these. mirrors optical] y, with the u se of a HeNe laser. The choice of the optical path shown in Fig. 5, was motivated by the desire to have a convenient receiver layout geometry and to keep the elliptical mirror bounce. angle less than 40°, to reduce focus aberrations.

2.5. IF System

At 1.4 GHz, the. impedance presented by the pumped junction at the end of the RF choke. filter is transformed into a purely real impedance (-25 Q) by a 24 mm long section of SO-Q coaxial transmission line. To calculate the. required length, the complex impedance in the. reference plane of the mixer block output connector has been evaluated from both calculations using a microwave CAD software [23], and network analyzer measurements on the actual mixer. These measurements were done at 4.2 K and for various bias voltages, allowing us to vary the junction dynamic resistance. from 70 Ω to 500 Ω.

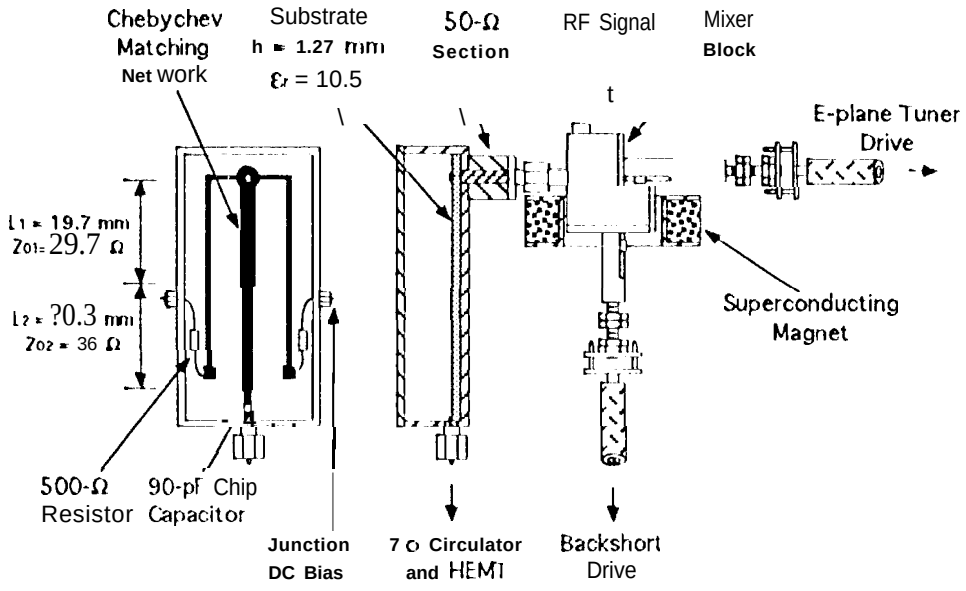

Fig. 6. Drawing of the two-section Chebychev microstrip IF transformer, of the. mixer block, and of' the, superconducting magnet.

A matching network then transforms the real impedance into 50 Ω, to match the impedance. of the cooled low-noise amplifier (I .NA). "l'his matching network, sketched in Fig. 6, is a microstrip two-section Chebychev transformer printed cm 1.27 mm thick *Duroid* (ε_r = *10.5)* substrate. For an assumed junction IF impedance (i.e., the dynamic resistance of the photon step at the. bias point) of 100 Q, this circuit provides a reflection coefficient at the transformer output lower than -15 dB over a 700-MHz bandwidth. A chip capacitor in the IF line serves as IX-block, and the DC leads appear to the matching network as very high IF impedance ports.

The LNA is a 3-stage HEMT (High Electron Mobility Transistor) amplifier from Berkshire Technologies [24], cooled to 13 K. The amplifier gain and noise temperature, specified at 77 K, are 33 dB and 5-6 K over nearly 800 MHz of bandwidth centered at 1.4 GHz. A circulator having its third port terminated by a 50-Ω resistor provides about 2.0 dB of isolation

between the IF matching circuit and the LNA. The measured bandwidth for the IF system is 500 MHz.

2.6. Cryogenics

The mixer and the optics are mounted to a 4-liter liquid helium tank, which cools the components to about 4.5 K by thermal conduction. in addition, a closed-cycle helium cryogenerator [25] cools two concentric jackets surrounding the helium tank down to 13 K and 80 K.

The LNA is heat-sunk to the 13-K station, All wires and coaxial cables are heat-sunk to the three stations on their way to the ambient temperature outer jacket. 'J'he copper wires which carry a significant fraction of an ampere to the magnet are heat-sunk to 4.5 K at the connection with the superconducting wires, to prevent any Joule effect in the copper from driving the magnet normal. The mechanical drives for the adjustable backshorts also contribute a significant heat flow. To reduce this contribution, they incorporate long sections of hollow epoxy rods, and the rotating couplers to the waveguide drives arc designed for a poor thermal contact: each coupler consi sts of a fork, with stainless steel pins which closely fit the holes of a thin brass plate (see Fig. 6). Under typical operating conditions, the measured receiver hold time is about 5 days.

3. Results ant] Discussion

3.1. Receiver Performance

Figure 7 summarizes the receiver performance as a function of LO frequency. The results labelled "Ml" are. for the in-house waveguide mount and a junction with the radial stub RF short; the "M2" results are for the second waveguide mount and a junction with the straight microstrip RF short. in addition, for the M2 results, a cooled HEMT amplifier with a factor 2 lower noise was used. The receiver noise power per unit bandwidth is expressed in temperat urc units for convenience using the Rayleigh-Jean's formula $P/B = kT$. The receiver has a double-sideband (DSB) response. For each point, the adjustable backshort and E-plane tuner, the 1.0 power, the bias voltage and the magnetic field have been optimized. The frequency range of the receiver is only determined by the LO frequency range. The best noise temperature is 245 K ± 15 K at 610 GHz for M2. The frequency response is relatively flat and the noise rises to only 330 K ± 19 K at 635 GHz. For M 1, the lowest noise

temperature. is 250 K ± 17 K, and the highest is 508 K ± 30 K at 635 GI lz. The rise in the noise temperat ure near 635 GI lz may indicate the edge of the mixer tuning range, determined by both the waveguide tuners and the integrated tuning circuit (The same junction has been measured in a scaled version of this receiver at 547 GHz, and those results [7] display a slightly different roll-off for the. receiver bandwidth). The variations of T_R across the IF bandwidth have also been measured for Ml, with a tunable 40-MHZ bandpass filter. As can be seen in Fig. 8, the receiver noise. varies smoothly within the IF bandwidth, The sharp increases near 1.05 GHz and 1.65 GHz correspond to the edges of the isolator bandwidth.

We derive T_R using the '}'-factor' method, i.e., from the relation

$$T_R = (T_h - Y T_c) / (Y - 1) \qquad (4)$$

where Y is the. ratio P_h/P_c of the IF output powers measured in response to a hot (T_h = 295 K) and a cold (T_c = 82 K) *Eccosorb* load placed at the receiver RF input. Near 600 GHz, to approximate the power radiated by these loads by the Rayleigh-Jean expression may lead to errors of about 15%. Therefore one has to use the complete Planck formula for blackbody radiation $P(T) = hfB / [\exp(hf/kT) - 1]$.

The integrated tuning circuit has been designed to optimize the mixer at 626 GHz. To investigate the. actual circuit resonance, we. have measured in the *I-V* characteristic the voltage of the step induced by the interaction of the AC Josephson current with the integrated circuit. At a bias voltage. *V,* the Josephson currents in the junction oscillate at frequency $f = (2e/h)$ V, and excite the strongly coupled microstrip resonator. in the absence of an external circuit, these currents would be shunted by the junction capacitance at any frequency higher than the plasma frequency (140 GHz for this particular junction). Nevertheless, whenever the junction and the. circuit resonate, all the AC currents arc self-absorbed in the junction and are responsible for a DC current step with a Lorentzian profile. One can thus usc the S1S junction, swept in voltage, to gather information on the circuit response [9,26,2.7], From such measurements, the resonance. seems to actually occur near 580 GHz for the junction with the. radial microstrip stub. Uncertainties in the magnetic penetration depth in the niobium electrodes and/or in the junction capacitance, and also effects of the quantum suscept ante [28], could account for the. frequency difference. For the. junction with the straight microstrip RF short, the resonance. occurs near 610 GHz. This frequency is closer to the. design frequency and this may account for the better performance. of M2.

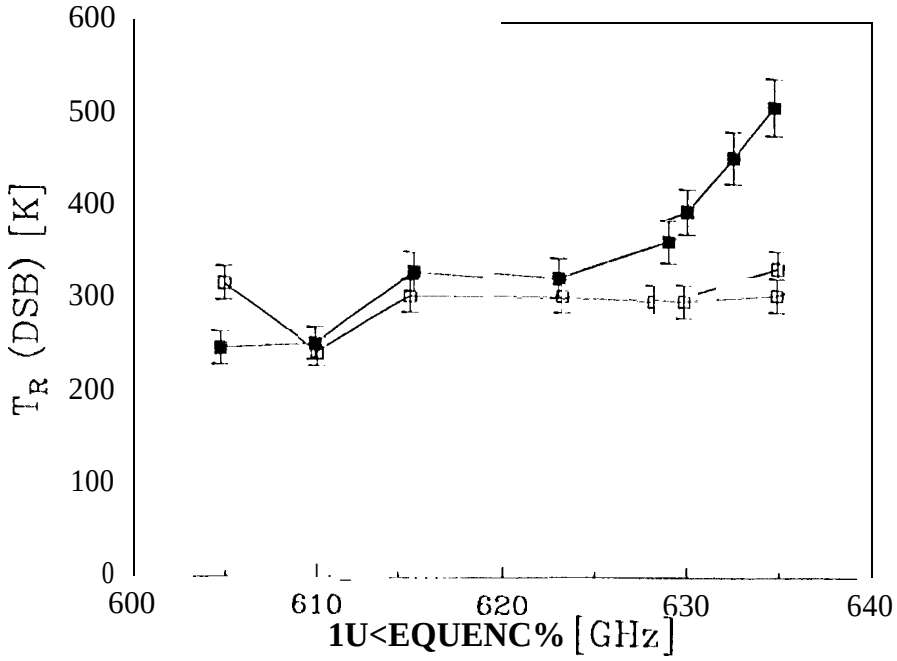

Fig. 7. Double-sideband receiver noise temperature versus LO frequency. The filled and empty squares correspond to the mixers "Ml" and "M2" respectively (see section 3.1. for discussion).

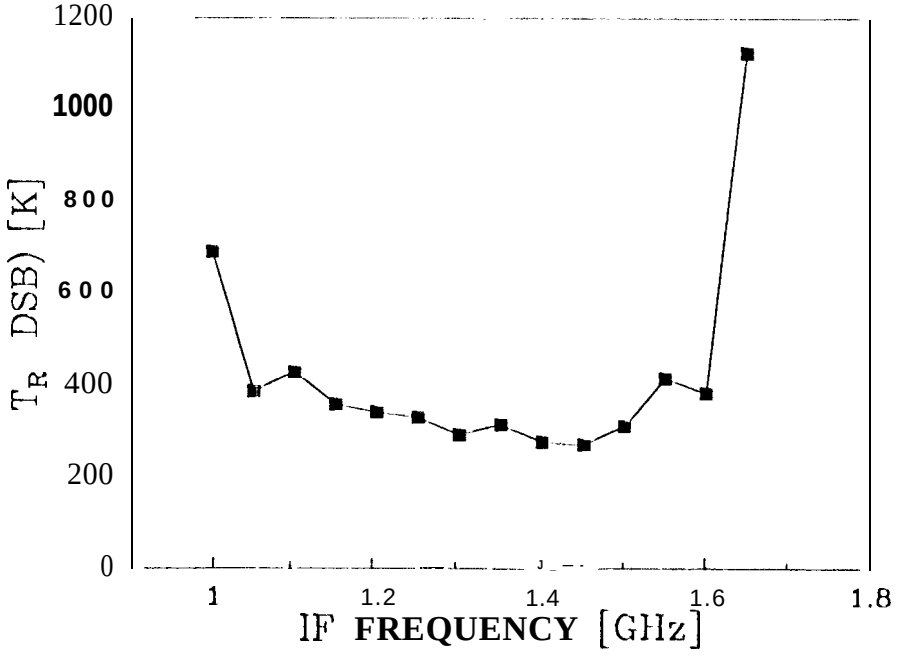

Fig. 8. Receiver noise temperature for mixer M 1 versus IF frequency, measured with a tunable 40-MHz bandpass filter.

We have estimated the noise and coupled conversion gain of M 1 at several frequencies, using the measured IF output power and subtracting the IF noise contribution. At 610 GHz (T_R = 250 K), one finds T_m' = 80 K and G_m' = 0.13 (-8.6 dB), where T_m' and G_m' include the effect of RF losses in the infrared filters, windows, diplexer, and mirrors. Similarly, at 635 GHz (T_R = S05 K), T_m' = *250* K and G_m' = 0.04 (-13.9 dB). The computed IF noise was obtained from shot noise measurements (see section 3.3). In the absence. of independent transmission and reflection measurements for the optical components, we cannot estimate the RF losses and their contribution to the noise accurately at the moment, although we expect that they may be significant,

3.2. Optimum DC Bias Voltage

Figure 9 shows the t ypical IF power response of the. receiver for the hot and cold loads, as a function of bias voltage. The corresponding pumped and unpumped *I-V* characteristics are also shown, The. best receiver noise was obtained at the higher voltage end of the photon step, that is, above the large dip that can be seen in the. IF output power curve. We believe this dip results from an overlap of the first-order photon step of the positive voltage region with the second-order photon step of the opposite (negative) voltage region. The latter decreases the pumped current in the region of overlap, causing a readily observable depression in the photon step. 'l"his effect is systematically and clearly seen in all *I-V* curves at high LO power levels. Furthermore, its dependence versus LO frequency and 1.0 power supports this interpretation, That is, the position of the depression is a linear function of the photon step width *hf/e*, and for sufficientl y high LO powers, a similar depression can be detected above the gap, seemingly involving the *third order* negative photon step. This effect is predicted by Tucker theory and has been observed in Al-based junctions at 73 GHz [29]. To our know] edge, however, there has been little experimental investigation of how this might affect the performance of a subrnillimemr-wave receiver. We. have thus thoroughly measured the increase in receiver noise in the region of the overlap for several frequencies and 1.0 power levels. Typicall y, when the mixer is optimized, the noise is higher than at bias voltages outside the overlap region by (10 - 40) %. This is a significant reduction in performance.

The photon step overlap described above has practical consequences for submillimeter wave receivers. In niobium-based junctions, the voltage range where. the. optimum mixer performance can be obtained is restricted to only a small fraction of the photon step. As the LO

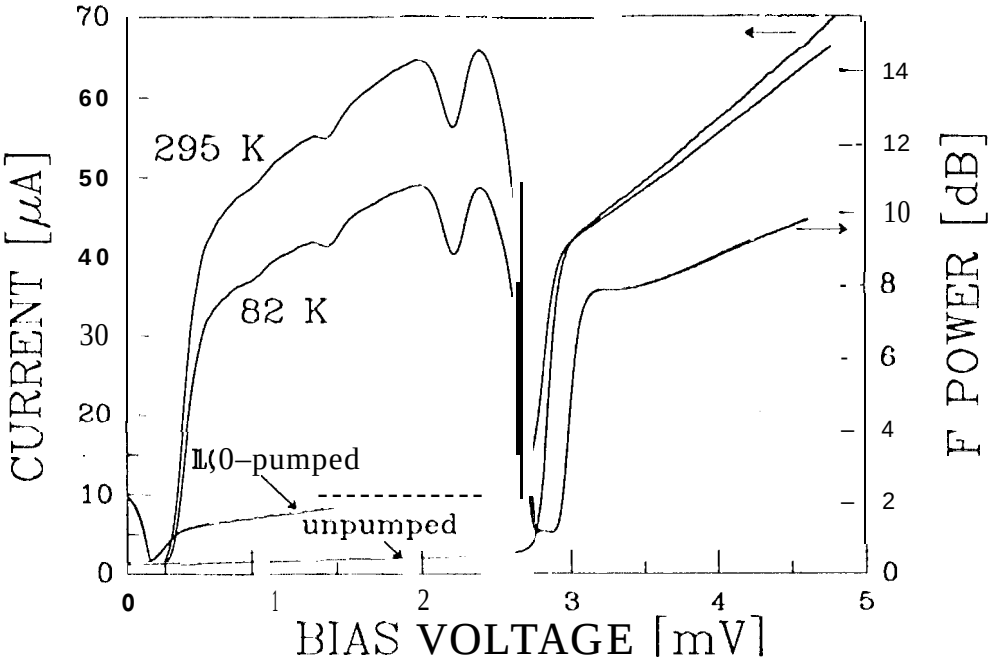

Fig.9. Typical IF output power versus bias voltage, for a hot (295 K) and a cold (82 K) load presented to the receiver input (mixer Ml). Superimposed are the unpumped, and the corresponding 1.()-pumped, *I-V* characteristics.

frequency approaches the energy gap frequency, this region further shrinks, reduced to a very narrow peak and eventually disappears. At frequencies above the energy gap frequency, while S1S mixers are still expected to perform reasonably well [30-32], the response degrades due to the fact that there is no best operating bias point left.

We emphasize another negative consequence of this overlap, which appears at 600 GHz for the all-niobium junctions. By an unfortunate coincidence, the best response bias region is located exactly near the second Shapiro step. Although the suppression of the Shapiro steps is, in theory, possible at any frequency by the application of a suitable magnetic field, this approach bccomcs more difficult to apply in practice, as one goes to the high submillimeter-wave frequencies. One flux quantum does average out the DC Josephson current, but it is not clear how well it averages out the AC counterpart: a perfectly smoothed *I-V* characteristic does not imply the perfect elimination of the Josephson noise at the IF frequency. The averaging process may be more efficient for a large number of applied flux quanta, but then, the field can be so strong that it reduces

the gap voltage of the junction, which further reduces the desirable DC bias voltage range. In addition, we have observed that the flux trapped in certain ultrasmall and high current density junctions is metastable. Together, these considerations make it preferable to bias far away from a Shapiro step, and may be incentives to use higher energy gap materials, such as NbN, for still higher frequencies.

3.3. IF System Noise

The noise of the complete IF system used with mixer M 1 was measured using a variable-temperature load method [33], where a well-matched resistive load is used as a variable source of thermal noise. The load has been connected to the. input of both the LNA and the IF matching network, These measurements confirmed the expected noise contribution from the combined LNA and room temperature amplifiers, of 6.5 K ± 0.5 K.

in the course of routine receiver operations, the IF noise is checked using the junction itself, biased at voltages above the gap voltage, as a variable noise source. 1 n the linear resistive branch of the I-V characteristic, $eV >> kT$ and the junction behaves as a source of shot noise power, at any bias current I:

$$P_{\text{shot}} = 2\, I\, e\, B_{\text{IF}}\, R_{\text{N}}\, C_{\text{IF}} \equiv kT_{\text{shot}}\, B_{\text{IF}} \qquad (5)$$

C_{IF} the IF coupling efficiency, which depends on the dynamic resistance R_{N} and on R_{o} the impedance presented to the junction by the. matching transformer:

$$C_{\text{IF}} = 4\, R_{\text{N}}\, R_{\text{o}} / (R_{\text{N}} + R_{\text{o}})^2 \qquad (6)$$

The total IF power measured over the bandwidth B_{IF} is

$$P_{\text{IF}} = k[T_{\text{shot}} + T_{\text{IF}}]G_{\text{IF}}B_{\text{IF}} = k[T_{\text{shot}} + (1-C_{\text{IF}})T_{\text{cir}} + T_{\text{LNA}}]G_{\text{IF}}B_{\text{IF}} \qquad (7)$$

where T_{cir} is the. physical temperature of the. circulator matched port. Hence, plotting P_{IF} versus I gives a straight line and the intersection with the. I-axis gives T_{IF}. Although T_{LNA} is constant, T_{IF} varies as the mixer is biased at various voltages, due. to the small amount of thermal radiation from the circulator load which is reflected back toward the amplifier. Therefore, most of the. uncertainties in the 'shot noise' method reside in the coupling efficiency achieved by the IF matching transformer. This transformer has been designed assuming a dynamic resistance for the

photon step near 150 Ω. However, current experimental data show that this resistance is much larger. In our case, $T_{LNA} \approx 6.5$ K was measured, but the total T_{IF} is often larger by typically 1.5 K due the impedance mismatch on the photon step.

3.4. Observations at the CSO

This receiver has been installed at the Cassegrain focus of the 10.5-rn CSO telescope, on Mauna Kea in Hawaii, for two separate one-weck periods. The first installation in early August was characterized by an atmospheric attenuation of nearly 20 dB at zenith angle (quite common for that time of the year) which severely hindered the observations. 'l'he later run in November was more fruitful due to exceptionally good weather, and allowed the detection of HCl and of other molecules in several astronomical objects. Figure 10 displays a spectrum of the molecular cloud Orion IRC2, and clearly shows the three hyperfine components of the $H^{35}Cl$ (J=1-O) transition at 625.92 GHz. For a double-sideband receiver noise temperature on site of 250 K - 350 K, the system noise temperature, which is dominated by the atmospheric attenuation, ranged from 2.000 K to 10,000 K DSB, varying with frequency, day, and zenith angle.

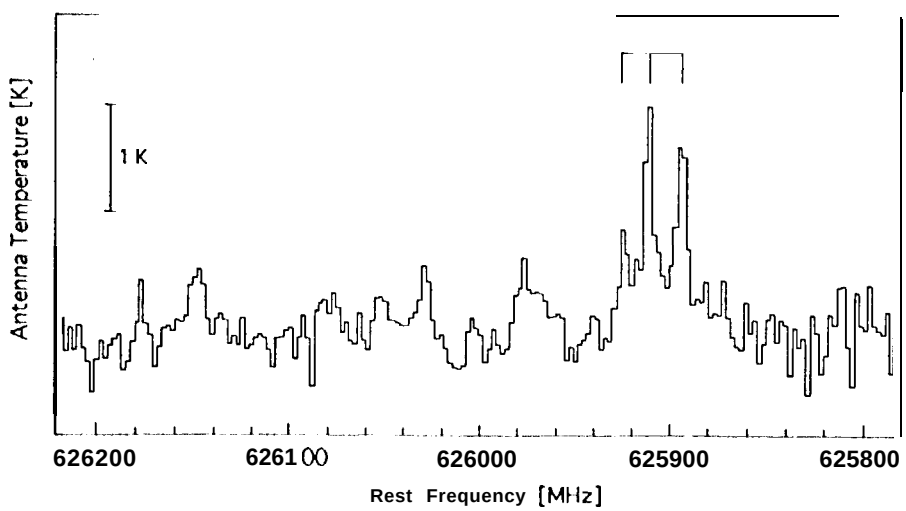

Fig. 10. Spectrum of Orion IRC2, for an integration time of 5 minutes (Tsys = 6550 K), showing the $H^{35}Cl$ (J=1-O) line at 625.92 GHz, with its three hyperfine components.

4. Conclusion

We have reported on the performance of' a waveguide S1S heterodyne receiver for use in the frequency range 600 Hz- 635 GHz. The lowest DSB noise temperature. of the receiver is 245 K. These results confirm that all-Nb junctions and tuning circuits can be employed in S1S receivers at signal frequencies as high as 90% of the energy gap frequency, At these frequencies, however, the second-order and first-order photon steps of opposite. voltage. regions overlap each other over a large fraction of the photon step where one expects good mixing performance, The receiver noise temperatures in and outside the overlap region may differ by 40%. Furthermore, the lower-noise part of the photon step is reduced to a small bias region, which is unstable because of its location near the second Shapiro step. The overlap of the photon steps will limit the performance of any S1S receiver using Nb at higher frequencies. This receiver has been successfully operated and used for astronomical observations at the CSO telescope, in Hawaii.

Acknowledgments

The research described in this paper was performed by the Center for Space Microelectronics Technology, Jet Propulsion I aboratory, California Institute of Technology, and was jointly sponsored by the Innovative Science and Technology Office of the Ballistic Missile Defense O~gani?.alien, and National Aeronautics and Space, Administration / Office of Advanced Concepts and Technology and the Office of Space Science. Morvan Salez and Pascal Febvre have been partly sponsored by Matra-Marconi Space, 3'OU1OU.SC, France., and DEMIRM, Observatoire de Meudon, France. Morvan Salez is currently sponsored by the Research Associateship Program of the National Research Council. Wc acknowledge, for their technical assistance at various stages of the receiver development: Dick Denning, Juergen Hernichel, Karl Jacobs, Mark Natzic, and in particular Joe Voeltz and Hardy Moham of JPL's Space. Instruments Machine. Shop, who fabricated most of the. receiver components. WC. also wish to thank Paul Batelaan, Gerard Beaudin, Robert Dengler, Michel Devoret, Hamid Javadi, Peter Siegel and Phillip Stimson for stimulating discussions and valuable advice. Wc also wish to thank the CSO staff for their generous assistance, and Tom Phillips for his continued support of this project

References

[1] B.N. Ellis on, P.]., Schaffer, W. Schaal, D. Vail and R.N. Miller, Internat. J. of Infrared and Millimeter Waves 10,937 (1 989).

[2] C.K. Walker, J.W. Kooi, M. Chan, H.G. LeDuc, P.L. Schaffer, J.E. Carlstrom and T.G. Phillips, *Proc. 3rd Internat. Symp. on Space Terahertz Technology,* p. *266,* University of Michigan, Ml (1992),

[3] J. Zmuidzinas and H.G. LeDuc, IEEE Trans. Microwave Theory and Techn. 40, 1797 (1992).

[4] J. Mees, G. DeLange, A. Skalare, C.E. Honingh, M. M.T.M. Dierichs, H. Kuipers, R.A. Panhuyzen, H. van de Stadt, M.W.M. de Graauw, and T.M. Klapwijk, *Proc. 18th Internat. Conf. on Infrared and Millimeter Waves,* p. 280, Colchester, U.K. (1993).

[5] J.R. Tucker, Appl. Phys. Lett. 36,477 (1980).

[6] B.N. Ellison, S.M.X. Claude, A. Jones, D.N. Matheson, L.T. Little and S.R. Davies, *Proc. 18th Internat. Conf. on Infrared and Millimeter Waves, p. 106,* Colchester, U.K. (1993).

[7] P. Febvre, W.R. McGrath, P. Batelaan, H.G. LeDuc, B. Bumble, M.A. Frerking and J. Hernichel, *Digest of IEEE MTT-S Internat. Microwave Symposium*, p. 771, Atlanta, GA (1993) ; *Proc. 18th Internat. Conf. on Infrared and Millimeter Waves,* p. *263,* Colchester, U.K. (1993).

[8] H.G. LeDuc, B. Humble, S.R. Cypher, A.J. Judas and J.A. Stern, *I'roe, 3rd Internat. Symp. on Space. Terahertz Technology*, p. 408, University of Michigan, MI (1992).

[9] A.V. Räisänen, W.R. McGrath, P.J.. Richards and F.L. Lloyd, IEEE Trans. Microwave Theory and Techn. **MTT-33**, 1495 (1985).

[10] Qing Hu, C.A. Mears and P.L. Richards, Phys. Rev. Lett. 64,2945 (1 990).

[11] B.A. Syrett, IEEE Trans. Microwave. Theory and Techn. **MTT-28**, 925 (1980).

[12] J.C. Swihart, 1961, J. Appl. Phys. 32,441 (1961).

[13] T.R. Gheewala, IBM J. Rcs. Develop. 24, 130 (1980).

[14] H.H.S. Javadi, W.R. McGrath, B. Bumble and H.G. LeDuc, Appl. Phys. Lett. 61,2712 (1 992).

[15] W.M. Chang, J. Appl. Phys. SO, 8129 (1979).

[16] H.M. Pickett, J.C. Hardy, J.C. and J, Farhoomand, IEEE Trans. Microwave Theory and Techn. **MTT-32**, 936 (1 984).

[17] Custom Microwaves inc., 940 Boston Ave, Longmont, CO.

[18] K. Jacobs and W.R. McGrath, *Digest of the 14th Internat. Conf. on Infrared and Millimeter Waves*, p. 539, Würzburg, Germany (1989).

[19] Radiometer Physics, Bergerwisen Straß 15, 53340 Meckenheim, Germany.

[20] Pacific Millimeter Products, 1890 Linbrook Drive, San Diego, CA.
[21] P.F. Goldsmith, Infrared and millimeter waves 6,277 (1982).
[2.2.] J.W. Iamb, Internat. J. of Infrared and Millimeter Waves 14,959 (1 992).
[23] Touchstone EEsof Inc., 5795 Lindero Canyon Road, Westlake Village, CA.
[24] Berkshire Technologies inc., $427 Telegraph Ave, Oakland, CA.
[25] CTI, 266 Second Ave, Waltham, MA.
[26] A. Larsen, H. Dalsgaard Jensen and J. Mygind, Phys. Rev. B 43, 10179 (1991).
[27] T. Hoist, D. Esteve, C. Urbina and M.H. Devoret, submitted to Phys. Rev. Letters (1994).
[28] A.H. Worsham, N.G. Ugras, D. Winkler, D.E. Prober, N.R. Erickson and P.F. Goldsmith, Phys. Rev. Lett. 67, 3034 (1991).
[29] D. Winkler and T. Claeson, J. Appl. Phys. 62,4482 (1 987).
[30] M.J. Feldman, Internat. J. of Infrared and Millimeter Waves 8, 12.87 (1987).
[31] W.C. Danchi and E.C. Sutton, J. Appl. Phys. 60,3967 (1 986).
[32] Tek-Ming Shen, IEEE J. of Quant. Electronics QE-17, 1151 (1981).
[33] W.R. McGrath, A.V. Räisänen and P. I.. Richards, Internat. J. of Infrared and Millimeter Waves 7,543 (1986).